Effects of Dissociation Relaxation upon Reflected Shock Waves and Unsteady Thermal Boundary Layers

By

Michinori MATSUSHITA* and Teruaki AKAMATSU*

(Received September 30, 1976)

Abstract

A numerical analysis was made for a dissociative reflected shock wave and its invicid flow field, and for unsteady thermal and concentration boundary layers developing at the end wall of a shock tube. It was shown that an entropy layer is formed adjacent to the end wall. The thermal boundary layer was found to have an overshoot of temperature which was sometimes higher than that outside the boundary layer. The concentration boundary layer was found to develop mainly due to the convection of highly dissociated gases from outside the boundary layer. It was found that self-similar boundary layers become valid finally.

Nomenclature

A : 4×4 matrix
a_f : frozen speed of sound
b_1 : constant
C : 4×4 matrix
D : diffusion coefficient
e : energy
f : column vector
h : enthalpy
K : thermal conductivity
k_{fN} : dissociation reaction rate coefficient by atom-molecule collision
k_{fN_2} : dissociation reaction rate coefficient by molecule-molecule collision
Ms : incident shock Mach number

* Department of Mechanical Engineering

p : pressure
Pr_0' : Prandtl number
q : heat flux
Q : artificial viscosity
Re_0 : Reynolds number
R_{N_2} : gas constant of nitrogen
Sc_0 : Schmidt number
T : temperature
t : time
Us : incident shock speed
v : velocity
w : column vector
x : distance from the end wall of a shock tube
z : column vector
α : degree of dissociation
$\dot{\alpha}$: rate of dissociation
γ : ratio of specific heats
θ_D : characteristic temperature for dissociation
η : non-dimensional coordinate

μ : viscosity coefficient
ρ : density
ρ_D : characteristic density for dissociation

Subscripts

0 : reference quantities
2 : behind incident shock wave
5 : behind reflected shock wave
F : frozen state
E : equilibrium state
' : dimensionless variables
∞ : outside of boundary layer

1. Introduction

After the incident shock wave reflected at the end wall of a shock tube, complicated phenomena, such as shown in Fig. 1, occur according to the interaction among the boundary layer at the end wall, the reflected shock wave and the dissociation relaxation. Intending to elucidate these phenomena, we will state two simplified problems in the following, so as to clarify the coupling effect between an unsteady

one dimensional flow and chemical reactions.

1) Reflection of a Dissociative Shock Wave at the End Wall of a Shock Tube

In this case the gas is assumed to be chemically reacting, invicid and non-conducting. The effects of all the transport processes are neglected in order to understand the basic features of a non-equilibrium dissociative reflected shock and its flow field. Nitrogen is adopted as the test gas and assumed to be Lighthill's ideal dissociating gas.

Employing the method of characteristics, Presley and Hanson[1] analysed the reflected shock and its flow field for chemically reacting oxygen. They concluded that the relaxation process behind a reflected shock wave exhibits two separate time scales controlled by the relaxation times behind the incident and reflected shock wave exhibits two separate time scales controlled by the relaxation times behind the incident and reflected shock waves. Also, adjacent to the wall, a variable entropy layer develops wherein the steady state values of all the thermodynamic variables, except pressure, differ significantly from their corresponding equilibrium values.

Employing the two step Lax-Wendroff method, we will obtain time varying profiles of the reflected shock and its flow field in detail. The virtue of this scheme is its simplicity, so that the calculation can proceed without any special treatment of a shock wave, using fixed rectangular mesh points. Adopting Lighthill's ideal dissociating gas, we can simplify the caloric equation of the state and the rate equation, and also reduce the computing time.

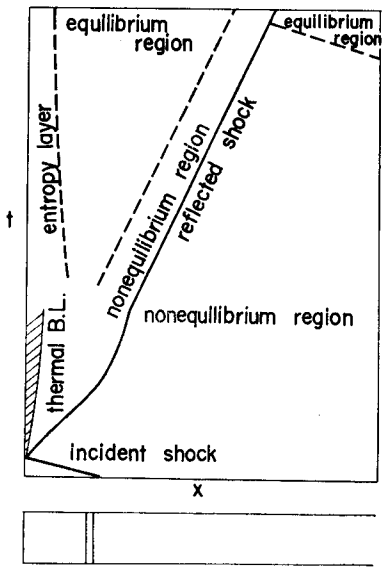

Fig. 1. x-t diagram of reflected shock and its flow field

2) Development of Dissociative Thermal and Concentration Boundary layers at the End Wall of a Shock Tube

In this case, we will observe the development of the boundary layers under the influence of a heat transfer and a diffusion to the end wall. Also to be observed is the advancement of the chemical reactions occuring in the gas phase and on the surface of the end wall. Putting aside the complicated problems of the interactions[3] between the reflected shock and the thermal boundary layer, we will consider the simplified situation that the hot gases immediately behind the shock wave suddenly contact the cold end wall of a shock tube. The hot gases are assumed to occupy a semi-infinite region and to be initially of the uniform frozen states given by the Rankine-Hugoniot frozen relations.

2. Reflection of a Dissociative Shock Wave at the End Wall of a Shock Tube

2.1 Basic Equations

Conservation equations of one dimensional, unsteady and chemically reacting flow including no transport phenomenon are as follows:

Mass: $$\frac{\partial \rho}{\partial t}+\frac{\partial}{\partial x}(\rho v)=0 \tag{1}$$

Momentum: $$\frac{\partial}{\partial t}(\rho v)+\frac{\partial}{\partial x}(p+\rho v^2)=0 \tag{2}$$

Energy: $$\frac{\partial}{\partial t}\left[\rho\left(e+\frac{1}{2}v^2\right)\right]+\frac{\partial}{\partial x}\left[\rho v\left(e+\frac{p}{\rho}+\frac{1}{2}v^2\right)\right]=0 \tag{3}$$

Atom: $$\frac{\partial}{\partial t}(\rho\alpha)+\frac{\partial}{\partial x}(\rho\alpha v)=\rho\dot{\alpha} \tag{4}$$

As the gas is assumed to be thermally perfect and ideally dissociating, the equations of state are as follows:

Thermal: $$p=(1+\alpha)\rho R_{N_2}T \tag{5}$$

Caloric: $$e=R_{N_2}(3T+\alpha\theta_D) \tag{6}$$

The rate equation of an ideal dissociating gas is

$$\dot{\alpha}=\left\{2\alpha\cdot k_{fN}+(1-\alpha)k_{fN_2}\right\}\frac{\rho}{w_{N_2}}\left(1-\alpha-\frac{\rho\alpha^2}{\rho_D}\cdot e^{\theta_D/T}\right) \tag{7}$$

$$k_{fN}=2.2\times10^{26}T^{-2.5}e^{-\theta_D/T} \tag{8a}$$

$$k_{fN_2}=3.9\times10^{33}T^{-4.5}e^{-\theta_D/T} \tag{8b}$$

These rate coe are given experimentally by Hanson and Baganoff[2] from the pressure history at the end wall of a shock tube.

Let us define the following dimensionless variables in terms of reference quantities: pressure P_0 and temperature T_0 in front of the incident shock wave, with the incident shock velocity $Us=Ms\sqrt{\gamma R_{N2}T_0}$ and the relaxation length behind the incident shock wave x_0,

$$p'=p/p_0 \qquad T'=T/T_0 \qquad v'=v/U_s \qquad \rho'=\rho U_s^2/p$$
$$x'=x/x_0 \qquad t'=tU_2/x_0 \qquad e'=e/U_s^2$$

where prime indicates dimensionless variables.

Dimensionless equations are as follows, where primes are abbreviated.

$$\frac{\partial w}{\partial t}+\frac{\partial f}{\partial x}=z \tag{9}$$

$$w=(\rho,\ \rho v,\ \rho\left(e+\frac{1}{2}v^2\right),\ \rho\alpha)^T$$

$$f=(\rho v,\ p+\rho v^2,\ \rho v\left(e+\frac{p}{\rho}+\frac{1}{2}v^2\right),\ \rho\alpha v)^T$$

$$z=(0,\ 0,\ 0,\ \rho\dot{\alpha})^T$$

$$p=(1+\alpha)\,\rho T/M_s^2\gamma \tag{10}$$

$$e=(3T+\alpha\theta_D)/M_s^2\gamma \tag{11}$$

The initial profiles for the incident shock wave and the relaxation region behind it are given by the steady state solutions of Eq. (9) evaluated by the RKG method. The end wall is assumed to be non-catalytic.

2.2 Finite Difference Equations

Replacing Eq. (9) by finite difference equations according to the two step Lax-Wendroff method given by Rubin and Burstein[4],

$$\overset{*}{w}{}_{j+\frac{1}{2}}^{n+1}=\frac{1}{2}(w_j^n+w_{j+1}^n)-\lambda(f_{j+1}^n-f_j^n)+\Delta t\cdot z_{j+\frac{1}{2}}^n \tag{12}$$

$$w_j^{n+1}=w_j^n-\frac{\lambda}{2}\left[\frac{1}{2}(f_{j+1}^n-f_{j-1}^n)+\left(\overset{*}{f}{}_{j+\frac{1}{2}}^{n+1}-\overset{*}{f}{}_{j-\frac{1}{2}}^{n+1}\right)\right]+\Delta t\cdot z_j^{n+\frac{1}{2}} \tag{13}$$

$$z_{j+\frac{1}{2}}^n=\frac{1}{2}(z_j^n+z_{j+1}^n) \qquad \overset{*}{f}{}_{j+\frac{1}{2}}^{n+1}=f(\overset{*}{w}{}_{j+\frac{1}{2}}^{n+1})$$

$$z_j^{n+\frac{1}{2}}=\frac{1}{2}\left[z_j^n+\frac{1}{2}\left(\overset{*}{z}{}_{j-\frac{1}{2}}^{n+1}+\overset{*}{z}{}_{j+\frac{1}{2}}^{n+1}\right)\right]$$

where subscripts j and n refer to the grid points on the x-t coordinates as shown in Fig. 2a. The truncation error of this scheme is $0(\Delta t^2)+0(\Delta x^2)$, and the stability condition is given by the CFL condition,

$$\lambda \leq \frac{1}{|v|+a_f} \tag{14}$$

where a_f is the frozen speed of sound in Lighthill gases:

$$a_f^2 = (4+\alpha)(1+\alpha)T/3$$

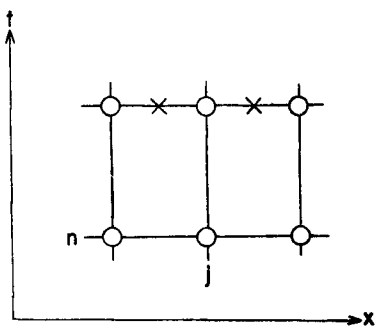

Fig. 2a. Grid points of difference scheme in sec. 2

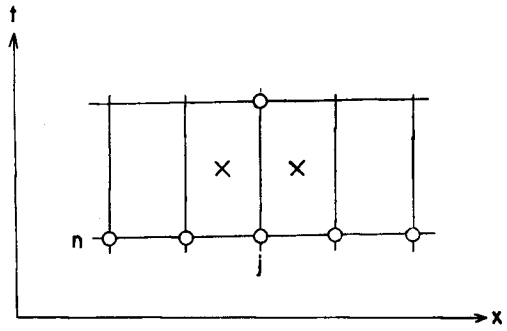

Fig. 2b. Grid points of difference scheme in sec. 3.

In order to stabilize the calculations and to dampen the oscillations behind the shock waves, we add the following viscosity term[5] of the von Neuman-Richtmyer type to the pressure terms in momentum and energy equations.

$$Q = -b_1 \rho \Delta x (|v|+a) \frac{\partial v}{\partial x} \tag{15}$$

The reflection method is employed as the boundary conditions at the end wall.

2.3 Results and Discussion

At first, the numerical computation was made for the case of an incident shock Mach number Ms=18 (Us=6km/sec), $p=1.0$ torr and $T=300°K$. We choose the mesh size $\Delta x=0.001$ and Courant number 0.9, then $\lambda=0.71$. The time varying profiles of density ρ, temperature α, degree of dissociation α and pressure p are shown in Fig. 3-6.

The frozen state immediately after the reflection, denoted by 2F5F, is given by the shock relations in Table 1. The gases in this frozen state relax rapidly into a dissociating state; α increasing, T and p decreasing and the reflected shock weakened. Then the velocity of the reflected shock wave becomes constant, and the following three regions are formed in the flow field: (1) the non-equilibrium relaxation region immediately behind the shock, (2) the variable entropy layer adjacent to the end wall, where the density is lower and the degree of dissociation is higher, (3) the flat region between the above-mentioned relaxation region and the entropy

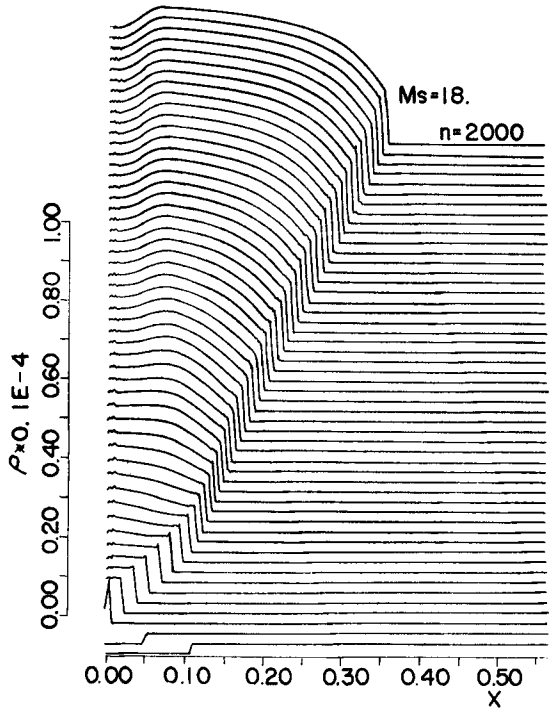

Fig. 3. Variation of density profiles (Ms=18).

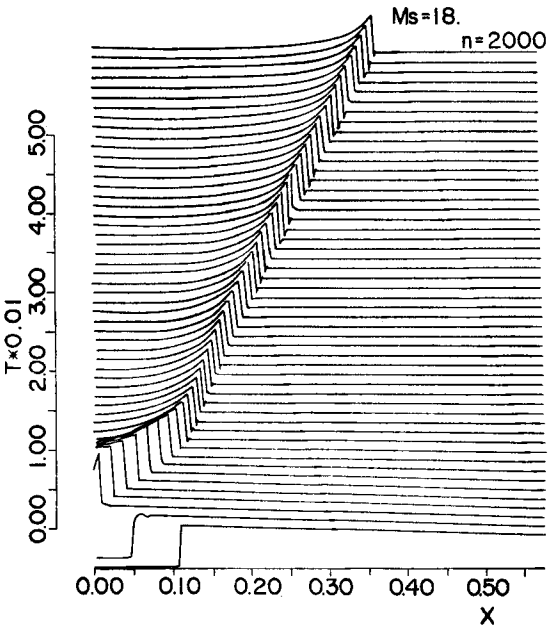

Fig. 4. Variation of temperature profiles (Ms=18).

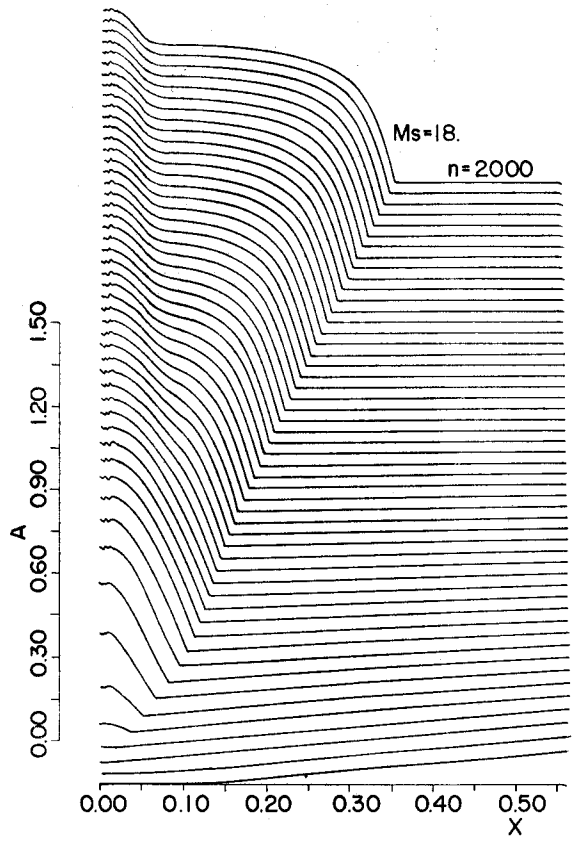

Fig. 5. Variation of degree of dissociation profiles (Ms=18).

layer. As the shock propagates farther from the end wall, the widths of the relaxation region and the entropy layer become constant and the flat region increases in width. The gas in the flat region relaxes toward the equilibrium state given by the equilibrium shock relation (2E5E) in Table 1. Comparing the state of the entropy layer with that of the equilibrium region at $n=4000$ ($t=2.9$), we will find that α amounts to 114% and ρ is equivalent to 86% of the values in the equilbrium region (see Table 2). This is attributed to the fact that the gas occupying the entropy layer passed the frozen shock which had not yet been weakened by the dissociation relaxation.

The properties at the end wall are shown in Fig. 7 as functions of time. Immediately after the reflection, the degree of dissociation increases and consequently, the temperature and the pressure decrease. Then, the pressure and the density increase gradually according to the increasing density in the relaxation region behind the

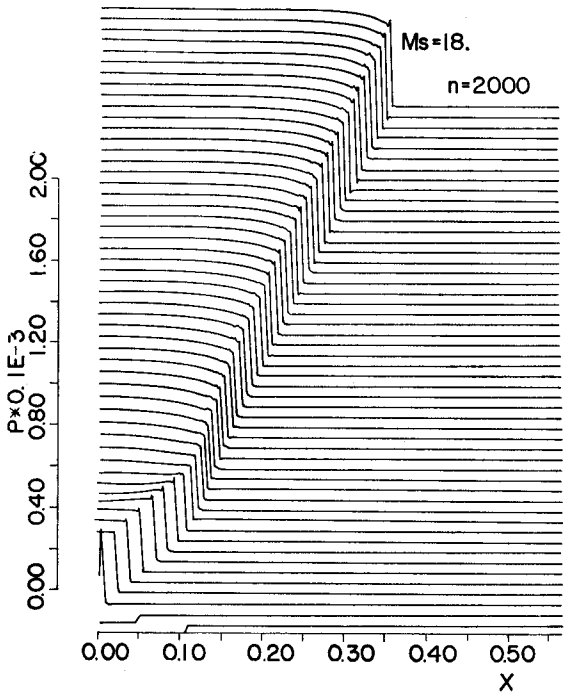

Fig. 6. Variation of pressure profiles (Ms=18).

Table 1 Shock relation.

Ms		α	T	p	ρ
18	2F5F	0.0	0.120×10^{3}	0.327×10^{4}	0.118×10^{5}
	2E5E	0.82	0.308×10^{2}	0.634×10^{4}	0.488×10^{5}
15	2F5F	0.0	0.835×10^{2}	0.225×10^{4}	0.809×10^{4}
	2E5E	0.52	0.263×10^{2}	0.365×10^{4}	0.274×10^{5}
12	2F5F	0.0	0.675×10^{2}	0.206×10^{4}	0.586×10^{4}
	2E5E	0.27	0.229×10^{2}	0.179×10^{4}	0.118×10^{5}

Table 2 Properties for the case of Ms=18 at n=4000 (t=2.9)

		α	T	p	ρ
Reflexion	wall	0.920	0.333×10^{2}	0.568×10^{4}	0.384×10^{5}
	eq. region	0.805	0.306×10^{2}	0.567×10^{4}	0.444×10^{5}
Isobaric		0.875	0.307×10^{2}	0.327×10^{4}	0.245×10^{5}
Isochoric		0.728	0.285×10^{2}	0.134×10^{4}	0.119×10^{5}

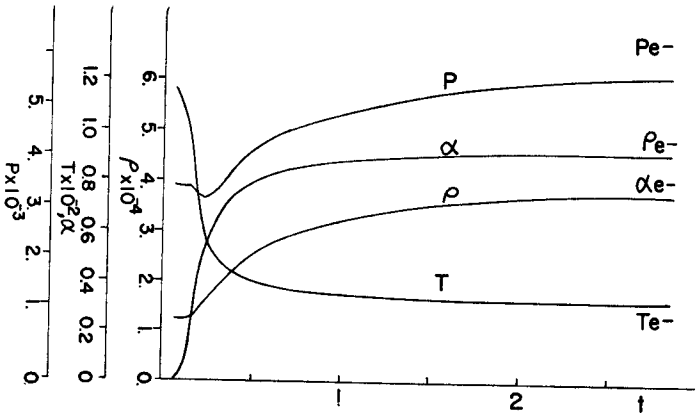

Fig. 7. End wall properties.

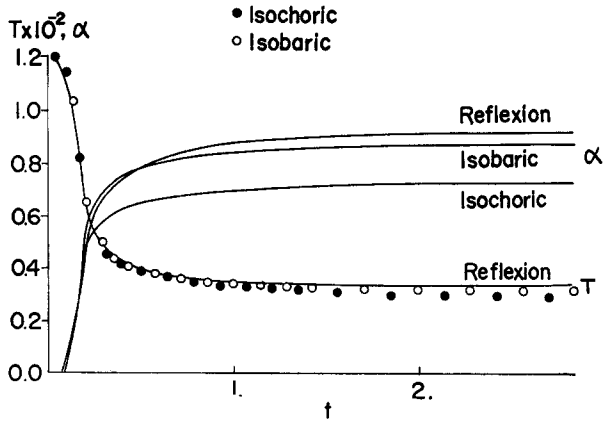

Fig. 8. Comparison of three relaxation processes.

incident shock. We can compare, in Fig. 8, this process with the virtual isobaric- and isochoric-relaxation processes that begin from the frozen state behind the reflected shock. Table 2 and Fig. 8 indicate that the actual variation of α is close to the isobaric process.

In the case of lower Mach numbers (Ms=12, 15), though the reflected shock paths become almost straight, entropy layers still clearly exist. (See Fig. 9-12)

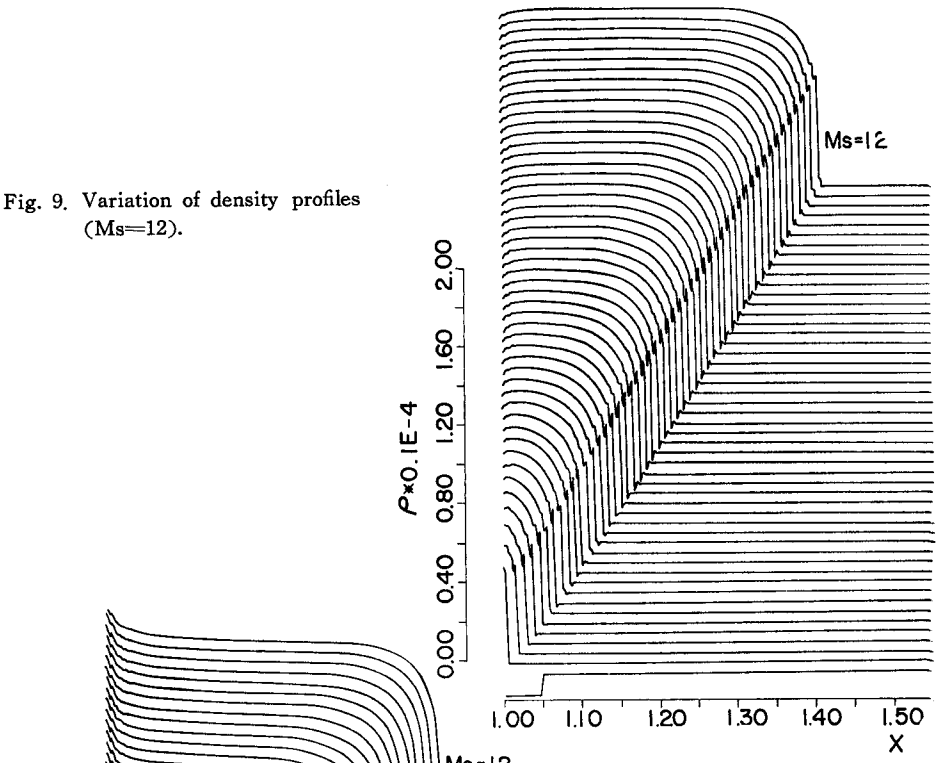

Fig. 9. Variation of density profiles (Ms=12).

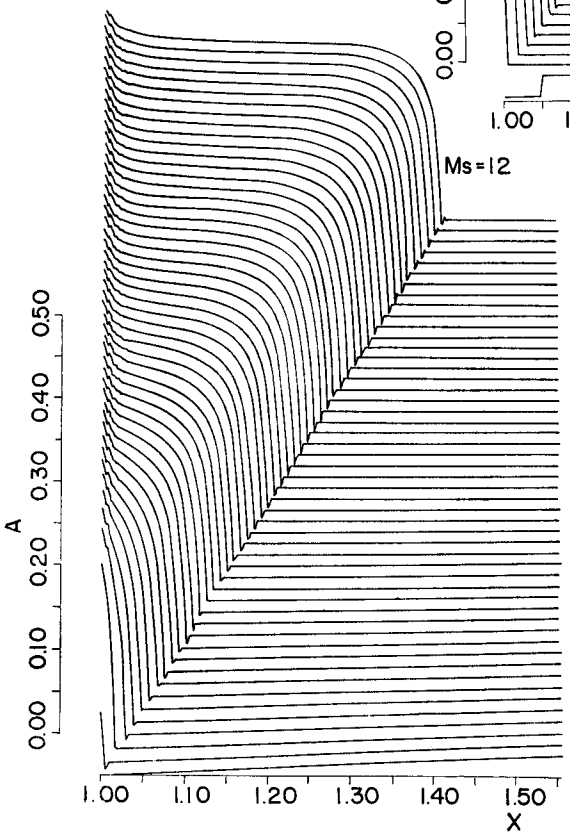

Fig. 10. Variation of degree of dissociation profiles (Ms=12).

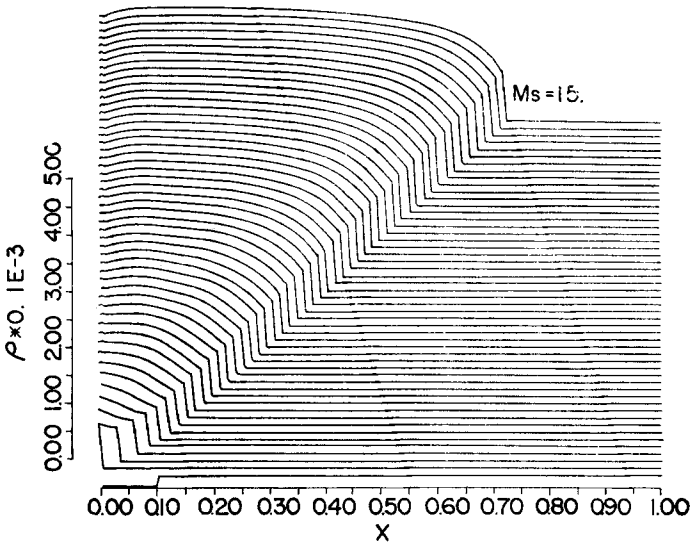

Fig. 11. Variation of density profiles (Ms=15).

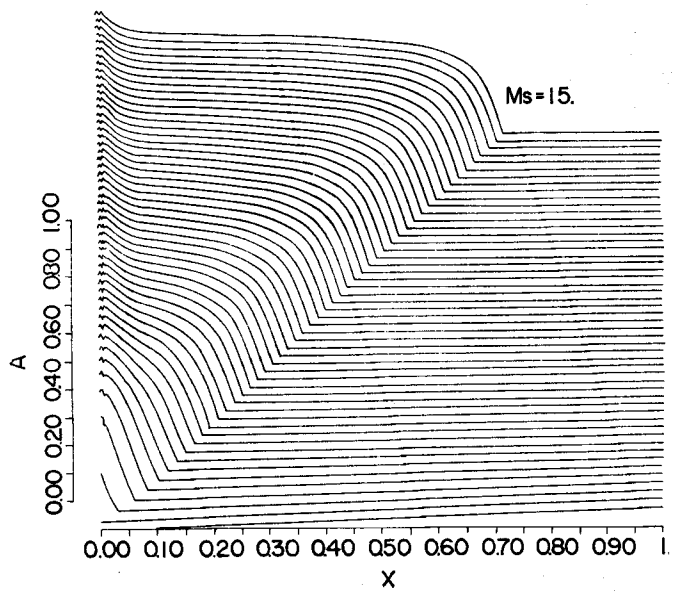

Fig. 12. Variation of degree of dissociation profiles (Ms=15).

3. Development of Dissociating Unsteady Thermal and Concentration Boundary Layers

3.1 Basic Equations

The chemically reacting unsteady one-dimensional Navier-Stokes equations are

$$\frac{\partial \rho}{\partial t}+\frac{\partial}{\partial x}(\rho v)=0 \tag{16}$$

$$\frac{\partial}{\partial t}(\rho v)+\frac{\partial}{\partial x}(p+\rho v^2)-\frac{\partial}{\partial x}\left(\frac{4}{3}\mu\frac{\partial v}{\partial x}\right)=0 \tag{17}$$

$$\frac{\partial}{\partial t}\left[\rho\left(e+\frac{1}{2}v^2\right)\right]+\frac{\partial}{\partial x}\left[\rho v\left(e+\frac{p}{\rho}+\frac{1}{2}v^2\right)\right]-\frac{\partial}{\partial x}\left[\frac{4}{3}\mu v\frac{\partial v}{\partial x}-q\right]=0 \tag{18}$$

$$\frac{\partial}{\partial t}(\rho\alpha)+\frac{\partial}{\partial x}\left[\rho\alpha\left(v-\frac{D}{\alpha}\frac{\partial \alpha}{\partial x}\right)\right]=\rho\dot{\alpha} \tag{19}$$

Heat flux q and viscosity coefficient μ are

$$q=-K\frac{\partial T}{\partial x}+\rho D\frac{\partial \alpha}{\partial x}\left[h_{N_2}-h_N\right] \tag{20}$$

$$\mu=\mu_0\left(\frac{T}{T_0}\right)^{0.75} \tag{21}$$

The equations of state and rate equation are the same as in section 2.

Let us define the dimensionless variables by employing the reference values in front of the incident shock wave: T_0, p_0, $v_0=\sqrt{R_{N_2}T_0}$, x_0 (mean free path of molecules) and $t_0=x_0/v_0$

Rewriting Eq. (16)-(19) by the dimensionless variables,

$$\frac{\partial \rho}{\partial t}+v\frac{\partial \rho}{\partial x}+\rho\frac{\partial v}{\partial x}=0 \tag{22}$$

$$\frac{\partial v}{\partial t}+v\frac{\partial v}{\partial x}+\frac{1}{\rho}\frac{\partial p}{\partial x}-\frac{1}{R_e\rho}\frac{\partial}{\partial x}\left(\frac{4}{3}\mu\frac{\partial v}{\partial x}\right)=0 \tag{23}$$

$$\frac{\partial e}{\partial t}+v\frac{\partial e}{\partial x}+\frac{p}{\rho}\frac{\partial v}{\partial x}-\frac{1}{R_e\rho}\left[\frac{4}{3}\mu\left(\frac{\partial v}{\partial x}\right)^2-\frac{\partial q}{\partial x}\right]=0 \tag{24}$$

$$\frac{\partial \alpha}{\partial t}+v\frac{\partial \alpha}{\partial x}-\frac{1}{\rho R_e S_c}\frac{\partial}{\partial x}\left(\rho D\frac{\partial \alpha}{\partial x}\right)=\dot{\alpha} \tag{25}$$

where $Re_0=\dfrac{\rho_0 v_0 x_0}{\mu_0}$ $Pr_0'=\dfrac{R_{N_2}\mu_0}{K_0}$ $Sc_0=\dfrac{\rho_0 D_0}{\mu_0}$

Assuming that the Prandtl number and the Schmidt number in the flow field are constant, we obtain

$$\mu=K=\rho D=T^{0.75} \tag{26}$$

The end wall is assumed to be isothermal, perfectly catalytic and impermeable. The initial conditions are given by discontinuous profiles:

$$x=0\ ;\ T=T_w,\quad \rho=\rho_{2f_5f},\quad p=\rho_{2f_5f}\times T_w,\quad v=\alpha=0$$

$$x>0\ ;\ T=T_{2f_5f},\quad \rho=\rho_{2f_5f},\quad p=p_{2f_5f},\quad v=\alpha=0$$

3.2 Finite Difference Equations

Writing the preceding partial differential equations in vector form, we obtain

$$w_t+Aw_x+\frac{1}{R_e}(cw_x)_x=z \tag{27}$$

According to the two step Lax-Wendroff method given by Thommen,[4] the finite difference expressions of Eq. (27) are

$$\overset{*}{w}{}^{n+\frac{1}{2}}_{j+\frac{1}{2}}=\frac{1}{2}(w^n_j+w^n_{j+1})+\frac{\lambda}{2}(A^n_{j+1}w^n_{j+1}-A^n_jw^n_j)+\frac{\Delta t}{4}(z^n_j+z^n_{j+1})$$

$$+\frac{\lambda^2}{4R_e\Delta t}\left[c^n_{j+\frac{1}{2}}(w^n_{j+2}-w^n_{j+1})-c^n_{j-\frac{1}{2}}(w^n_j-w^n_{j-1})\right] \tag{28}$$

$$w^{n+1}_j=w^n_j+\lambda(\overset{*}{A}{}^{n+\frac{1}{2}}_{j+\frac{1}{2}}\overset{*}{w}{}^{n+\frac{1}{2}}_{j+\frac{1}{2}}-\overset{*}{A}{}^{n+\frac{1}{2}}_{j-\frac{1}{2}}\overset{*}{w}{}^{n+\frac{1}{2}}_{j-\frac{1}{2}})+\frac{\Delta t}{2}(\overset{*}{z}{}^{n+\frac{1}{2}}_{j+\frac{1}{2}}+\overset{*}{z}{}^{n+\frac{1}{2}}_{j-\frac{1}{2}})$$

$$+\frac{\lambda^2}{R_e\Delta t}\left[c^n_{j+\frac{1}{2}}(w^n_{j+1}-w^n_j)-c^n_{j-\frac{1}{2}}(w^n_j-w^n_{j-1})\right] \tag{29}$$

$$c_{j\pm\frac{1}{2}}=\frac{1}{2}(c_{j\pm1}+c_j)$$

where the subscripts j and n refer to the grid points on the x-t coordinates as shown in Fig. 2b. The truncation error of this scheme is $0(\Delta t^2)+0(\Delta x^2)+0(\Delta t/R_e)$. Hence, if we set $\Delta t=0(1/\mathrm{Re})$, the entire scheme formally has a second order accuracy.[6]

The boundary values for T, α and v at the end wall are given by the physical assumptions that the end wall is isothermal, perfectly catalytic and impermeable. The other boundary values are determined by linear extrapolations.

3.3 Results and Discussion

A numerical computation was made for the case of an incident shock Mach number Ms=12, $T_0=300$°K, $p_0=1.0$torr and $x_0=0.05$mm with the mesh size $\Delta x=0.05$, $\Delta t=0.001$, then $\lambda=0.02$. Following the conventional analysis of a non-reacting thermal boundary layer, we now introduce a new variable:

$$\eta=\frac{\int_0^x\rho dx}{2\sqrt{p_\infty t}}$$

Temperature- and pressure-profiles normalized by the values outside the boundary

layer at each instant are shown in Fig. 13 and 14. The heat transfer to the cold end wall yields the thermal boundary layer. The rarefaction wave, induced by the flow toward the cold end wall, propagates outside the boundary layer.

There exists an overshoot of temperature behind the rarefaction wave and it is

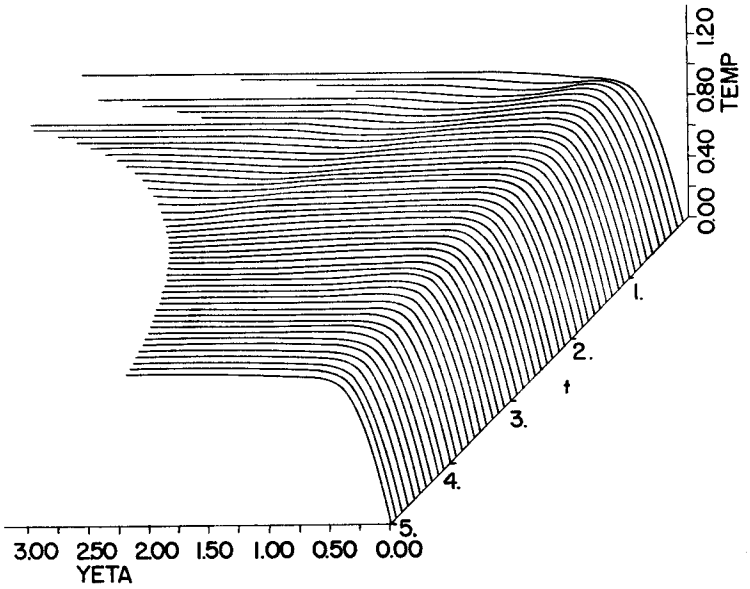

Fig. 13. Variation of temperature profiles.

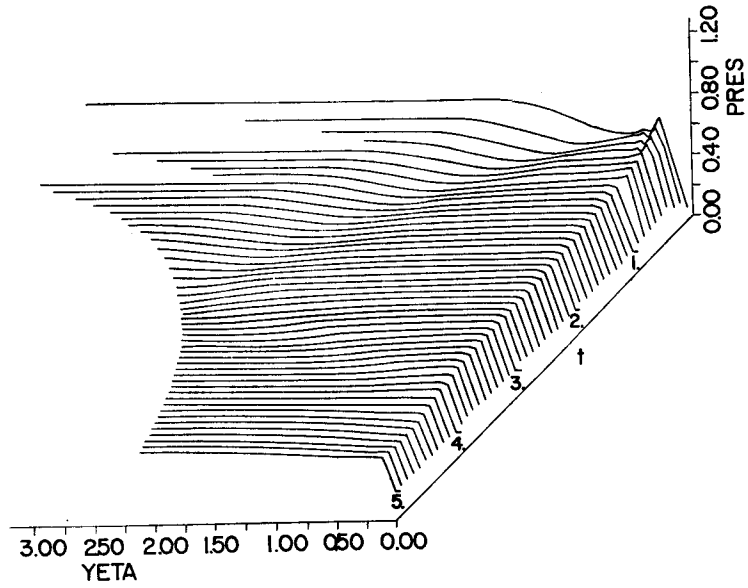

Fig. 14. Variation of pressure profiles.

found, in certain cases, that the temperature in some regions of the boundary layer becomes higher than the temperature outside the boundary layer. The physical explanation for this result is that the kinetic energy of the gas flowing toward the end wall is transferred into thermal energy due to the interception by the end wall.

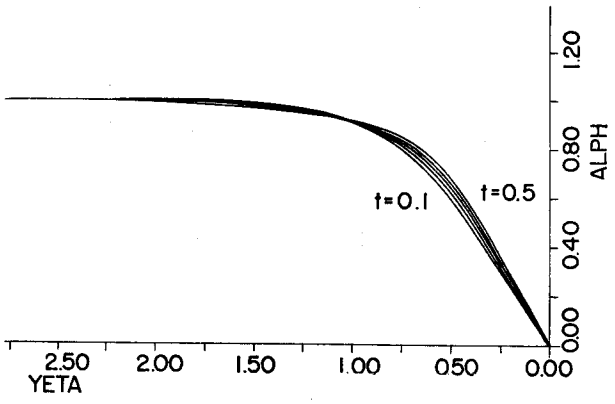

Fig. 15. Variation of degree of dissociation profiles.

The degree of dissociation normalized by the values outside the boundary layer is shown in Fig. 15. Figure 16 gives some explanation about the process that α increases gradually in the boundary layer. The time variations (at $\eta=0.5$) of the convection term (C), the reaction term (R) and the diffusion term (D) in the atom conservation equation (25) are shown in the figure. Considering that the convection term is greater than the reaction term at $t>0.1$, we can conclude that the increasing of α in the boundary layer is mainly due to the convection of highly dissociated gas from outside the boundary layer rather than the chemical reaction within the boundary layer. The minus sign in the diffusion term means that nitrogen molecules produced by the surface reaction on the end wall diffuse toward the outside of the boundary layer, and that consequently the concentration of atoms (degree of dissociation) decreases. Figures 17 and 18 indicate that the convection term is dominant near the wall, and that reaction term is dominant near the outer edge of the boundary layer.

The degree of dissociation outside the boundary layer amounts to 95% of the equilibrium value at $t=5$. Figures 16, 17 and 18 show that all the contributions due to the convection, reaction and diffusion attain almost a steady state at $\eta=$const, when $t=5$. Therefore, self-similar solutions are expressible in the term of η when $t=5$. Figure 17 indicates that the reaction rate is almost zero at $\eta=0.25$, that is,

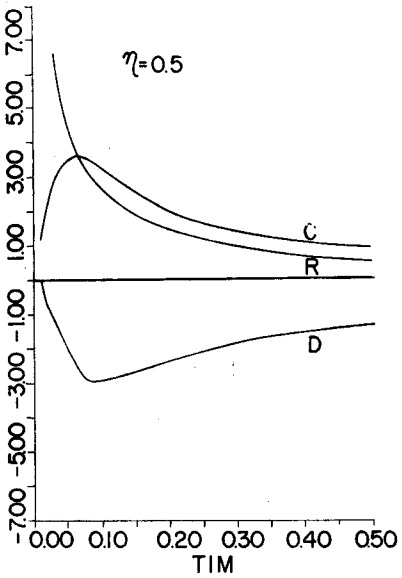

Fig. 16. Variation of three terms in atom conservation Eq. at η=0.5

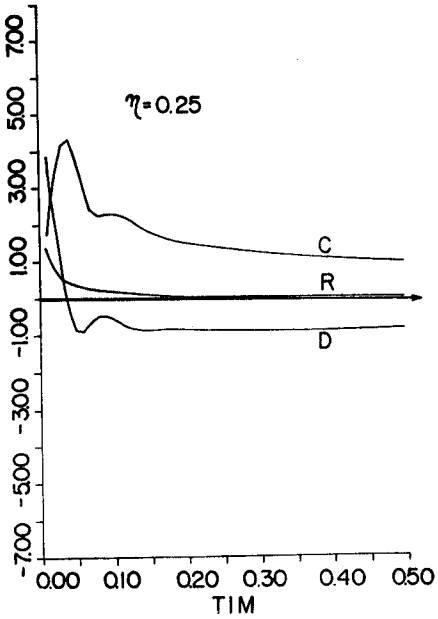

Fig. 17. Variation of three terms in atom conservation Eq. at η=0.25

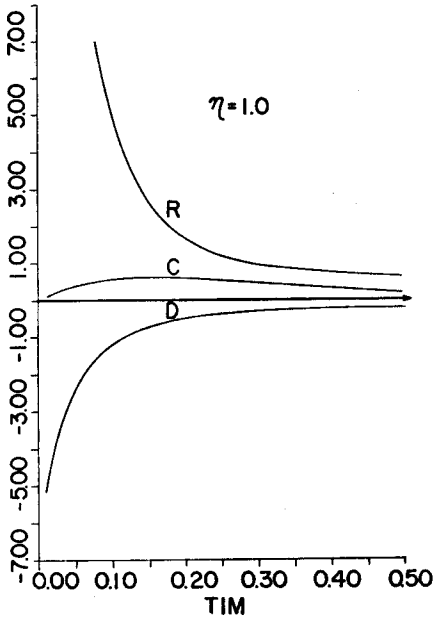

Fig. 18. Variation of three terms inatom conservation Eq. at η=1.0

gases near the wall are almost in equilibrium states. In general, the reaction term never becomes minus at any point in the boundary layer. This means that recombination reactions, which are exothermic, never go forward in spite of a cooling effect by the wall. These phenomena are explained in the following. The end wall being perfectly catalytic, molecules are produced at an infinite reaction rate by a recombination of atoms. Moreover, the characteristic time of a recombination reaction in the gas phase is not so short as that of the molecular diffusion. Therefore, the recombination reaction in the gas phase does not go forward, and the almost equilibrium state is maintained.

4. Conclusion

A numerical analysis was performed for the two phenomena associated with the interaction between the flow field behind the reflected shock and the non-equilibrium chemical reaction. In the analysis of the dissociative shock reflection a variable entropy layer was formed, where the final steady state was different from the equilibrium state given by a shock relation.

In the analysis of the unsteady thermal and concentration boundary layer, it was found that there existed an overshoot of temperature which was sometimes higher than the temperature outside the boundary layer. It was further found that the concentration boundary was developed mainly by the convection of a highly dissociated gas from outside the boundary layer. As the gas phase reaction approached the equilibrium state, the convection and diffusion balancing, and also the self-similar unsteady boundary layer developed. It takes too much time to calculate, by the present scheme, the shock reflection and the development of the boundary layers simultaneously for the purpose of studying the coupling between the entropy layer and the boundary layer.

In a case where the wall catalysity is finite, differing from that of the present case, we may find other interesting non-equilibrium phenomena. Instead of analysing full Navier-Stokes equations, we can introduce unsteady boundary layer equations employing the independent variables η in section 3.3. Considering the stability of the numerical scheme and the singularity of the boundary layer equations at $t=0$, we should analyse them by implicit finite difference methods.

The numerical calculations were carried out on FACOM 230-75 at the Data Processing Center in Kyoto University.

References

1) Presley, L. L. and Hanson, R. K., "Numerical Solutions of Reflected Shock-Wave Flowfields with Nonequilibrium Chemical Reactions," AIAA J., Vol. 10, 1969.

2) Hanson, R. K. and Baganoff, D., "Shock-Tube Study of Nitrogen Dissociation Rates Using Pressure Measurements," AIAA J., Vol. 10, 1972.
3) Clarke, J. F., "The Reflexion of a Plane Shockwave from a Heat-conducting Wall," Proc. Roy. Soc., A299, 1967.
4) Rubin, E. L. and Burstein, S. Z., "Difference Methods for the Invicid and Viscous Equations of a Compressible Gas," J. Comp. Phys., Vol. 2, 1967.
5) Roache, P. J., "Computational Fluid Dynamics," Hermosa Pub. Albuquerque, 1972.
6) Palumbo, D. J. and Rubin, E. L., "Solutions of Two Dimensional Unsteady Compressible Navier-Stokes Equations using Second-Order Accurate Numerical Scheme," J. Comp. Phys Vol. 9. 1972.
7) Vincenti, W. G. and Kruger, Jr., C. H., "Introduction to Physical Gas Dynamics," John Wiley and Sons, Inc., 1965.